Inorganic Chemistry

Article

pubs.acs.org/IC

Cation Miscibility and Lithium Mobility in NASICON $Li_{1+x}Ti_{2-x}Sc_x(PO_4)_3$ ($0 \leq x \leq 0.5$) Series: A Combined NMR and Impedance Study

Radhouene Kahlaoui,[†] Kamel Arbi,[*,‡,§] Isabel Sobrados,[‡] Ricardo Jimenez,[‡] Jesus Sanz,[‡] and Riadh Ternane[†]

[†]Laboratoire d'Application de la Chimie aux Ressources et Substances Naturelles et à l'Environnement (LACReSNE), Université de Carthage, Faculté des Sciences de Bizerte, 7021 Zarzouna, Bizerte, Tunisia

[‡]Instituto de Ciencia de Materiales de Madrid (ICMM), Consejo Superior de Investigaciónes Científicas (CSIC), Cantoblanco, 28049 Madrid, Spain

[§]Department of Materials and Environment (Microlab), Faculty of Civil Engineering & Geosciences, Delft University of Technology, Delft, The Netherlands

ABSTRACT: Rhombohedral NASICON compounds with general formula $Li_{1+x}Ti_{2-x}Sc_x(PO_4)_3$ ($0 \leq x \leq 0.5$) have been prepared using a conventional solid-state reaction and characterized by X-ray diffraction (XRD), nuclear magnetic resonance (NMR), and impedance spectroscopy. The partial substitution of Ti^{4+} by Sc^{3+} and Li^+ in pristine $LiTi_2(PO_4)_3$ increases unit-cell dimensions and the number of charge carriers. In Sc-rich samples, the analysis of XRD data and $^6Li/^7Li$, ^{31}P, and ^{45}Sc MAS NMR spectra confirms the presence of secondary $LiScO_2$ and $LiScP_2O_7$ phases that reduce the amount of lithium incorporated in the NASICON phase. In samples with $x < 0.3$, electrostatic repulsions between Li ions located at M1 and M3 sites increase Li mobility. For $x \geq 0.3$, ionic conductivity decreases because of secondary nonconducting phases formed at grain boundaries of the NASICON particles (core−shell structures). For $x = 0.2$, high bulk conductivity (2.5×10^{-3} S·cm^{-1}) and low activation energy ($E_a = 0.25$ eV) measured at room temperature make $Li_{1.2}Ti_{1.8}Sc_{0.2}(PO_4)_3$ one of the best lithium ionic conductors reported in the literature. In this material, the vacancy arrangement enhances Li conductivity.

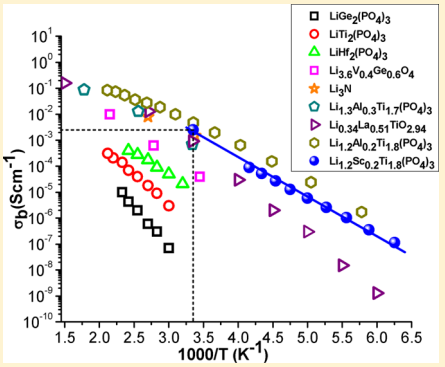

I. INTRODUCTION

Over the last decades, a wide variety of solid electrolytes with high ionic conductivities have attracted great interest for electrochemical applications.[1−3] Among different proposed materials, $LiM_2(PO_4)_3$ phosphates with a NASICON (acronym for sodium (Na) super ionic conductor) structure are being considered promising candidates to be used as electrodes and/or electrolytes in all-solid high-energy lithium batteries, because of their chemical stability and high Li mobility in three-dimensional conduction networks.[3−8]

In NASICON $LiM_2(PO_4)_3$ compounds, each $[PO_4]$ tetrahedron shares corners with four $[TiO_6]$ octahedra, and each octahedron shares oxygens with six tetrahedra. In $LiM_2(PO_4)_3$ ($M^{4+} = Ti^{4+}$, Ge^{4+}) phases, the structure displays rhombohedral symmetry (space group $R\bar{3}c$),[9,10] but in $LiM_2(PO_4)_3$ ($M^{4+} = Zr^{4+}$, Sn^{4+}, and Hf^{4+}) phases a triclinic distortion (space group $C\bar{1}$) was reported.[11−13] In rhombohedral $LiM_2(PO_4)_3$ phases, two crystallographic sites are possible for alkaline cations: M1 sites, located at ternary axes, are surrounded by six oxygens, and M2 sites, symmetrically distributed around a 3-fold axis, are 10-fold oxygen coordinated. In rhombohedral phases, the preferential occupancy of M1 sites has been reported.[10,11] However, in triclinic phases, Li cations are 4-fold coordinated at intermediate M12 sites.[12,13]

The partial substitution of Ti^{4+} by trivalent cations such as Al^{3+}, Sc^{3+}, Ga^{3+}, Fe^{3+}, In^{3+}, and Cr^{3+} in $Li_{1+x}R_xTi_{2-x}(PO_4)_3$ materials, is compensated by lithium, improving ion conductivity.[14−24] In these compounds, correlations between structure, preparation conditions, and densification of pellets have been previously reported. In particular, Aono et al.[14] reported high lithium conductivity at room temperature, 7×10^{-4} S·cm^{-1}, in $Li_{1.3}R_{0.3}Ti_{1.7}(PO_4)_3$ compounds ($R^{3+} = Al^{3+}$or Sc^{3+}). In Al-doped samples, Fourier map differences performed with neutron diffraction showed that Li ions occupy M1 and M3 sites. In these samples, location of vacancy at M1 sites enhances considerably the ion conductivity.[17] Very recently, Arbi et al.[23] extended the NMR and electric study to the $Li_{1.3+x}Al_{0.3}R_xTi_{1.7-x}(PO_4)_3$series ($R^{3+} = Sc^{3+}$, In^{3+}). The authors reported that the incorporation of additional Sc^{3+} or In^{3+} increases the amount of lithium in NASICON compounds and delays the formation of the secondary $AlPO_4$ phase. However, the increase of lithium does not significantly improve

Received: September 22, 2016
Published: January 9, 2017

DOI: 10.1021/acs.inorgchem.6b02274
Inorg. Chem. 2017, 56, 1216−1224

the Li conductivity in Sc- and In-doped $Li_{1.3}Al_{0.3}Ti_{1.7}(PO_4)_3$ samples.

The preparation of rhombohedral $Li_{1+x}R_xTi_{2-x}(PO_4)_3$ NASICON phases by a ceramic route has been extensively documented.[19−21] However, NMR studies of this series are scarce. In these compounds, the presence of different $P(OR)_n(OTi)_{4-n}$ components ($0 \le n \le 4$) in the ^{31}P MAS NMR spectra can be used to estimate chemical composition of rhombohedral samples[24] and $^6Li/^7Li$ MAS NMR spectroscopy to investigate sites and mobility of Li ions.[25]

For a better understanding of the compositional dependence on conductivity, the investigation of the NASICON $Li_{1+x}Ti_{2-x}Sc_x(PO_4)_3$ ($0 \le x \le 0.5$) series has been here performed. Structural features have been studied with X-ray diffraction (XRD) and NMR, and Li mobility followed with NMR and impedance spectroscopy (IS) techniques. The combination of all these techniques provides useful information about lithium conduction in NASICON compounds.

II. EXPERIMENTAL PROCEDURE

$Li_{1+x}Ti_{2-x}Sc_x(PO_4)_3$ samples have been prepared by solid-state reaction, according to the reaction

$$3(NH_4)_2HPO_4 + (2 - x)TiO_2 + x/2Sc_2O_3 + (1 + x)/2Li_2CO_3 \rightarrow Li_{1+x}Ti_{2-x}Sc_x(PO_4)_3 + 6NH_3 + 9/2H_2O + (1 + x)/2CO_2$$

Stoichiometric amounts of $(NH_4)_2HPO_4$ (Roth, >97%), TiO_2 (Aldrich, 98%), Sc_2O_3 (Aldrich, 99.9%), and Li_2CO_3 (Merck, >99%) were used. The reagents were first heated at 390 K for 10 h to remove any traces of water; then, they were mixed in an agate mortar and heated at 1173 K for 12 h in a platinum crucible[19,23] to obtain the NASICON compounds.

X-ray diffraction analyses of powder samples have been carried out with a Bruker D8-Advance diffractometer, using 1.5406 Å Cu−Kα1 radiation (40 kV and 30 mA). Data were collected in the 10−70 (2θ) interval, with 0.02° steps of 0.5 s counting time/step. Crystalline phases were identified using the International Centre for Diffraction Data (ICDD). Structural refinements were carried out with the Rietveld technique (FullProf program).[26,27] In refinements, a pseudo-Voigt function was chosen to describe the line shape of diffraction peaks. In the first stage, scale factors, background coefficients, 2θ zero positions, line widths, and peak shapes were determined. In a second stage, positional parameters, site occupations, and atom thermal factors were deduced.

$^6Li/^7Li$, ^{45}Sc, and ^{31}P NMR spectra have been recorded at room temperature in an AVANCE-400 Bruker spectrometer (9.4 T) working at 58.88/155.50, 97.20, and 161.97 MHz, respectively. In magic angle spinning (MAS) experiments, samples were rotated around an axis inclined 54°44′ with respect to the external magnetic field at 2 kHz for $^6Li/^7Li$ and 4 kHz for ^{31}P and ^{45}Sc signals. $^6Li/^7Li$ and ^{31}P NMR signals were recorded after $\pi/2$ (3 and 4 μs) and ^{45}Sc NMR signals after $\pi/8$ (1 μs) pulse irradiation. In all cases a recycling time of 15 s was used between accumulations. The number of scans was in the range 100−800. Chemical shifts of $^6Li/^7Li$, ^{45}Sc, and ^{31}P signals were given relative to aqueous LiCl (1 M), $Sc(NO_3)_3$ (1 M), and H_3PO_4 (85 wt %), solutions, respectively. The analysis of NMR spectra has been carried out with the Winfit software package (Bruker),[28] which permitted intensity, line width, and position of components to be determined. Chemical shift (δ_{iso}), quadrupolar constants (C_Q), and asymmetry parameter (η) values have been deduced with trial and error procedures.

Electrical measurements have been performed on cylindrical pellets (6 mm in diameter and 1.5 mm in thickness) obtained by applying a uniaxial pressure of 120 MPa. In all cases, the achieved density of pellets was above 85%. Samples were sintered at 1123 K for 12 h. Electrodes were deposited by sputtering gold on opposite faces of the pellets. Measurements have been performed under a vacuum atmosphere, with a 4L-configuration between 77 and 550 K (10 K intervals) in a JANIS VPF 750 cryostat under a vacuum atmosphere. An automatically controlled Agilent Precision LCR E4980-A analyzer was used for low-frequency measurements (20 Hz to 2 MHz). To extend the frequency range, an Agilent E4991-A RF impedance analyzer (1 MHz to 3 GHz) was used at room temperature, placing the sample at the device port between the inner connector and short-circuit cap.

III. RESULTS

1. Structural Refinements. XRD patterns of $Li_{1+x}Ti_{2-x}Sc_x(PO_4)_3$ ($0 \le x \le 0.5$) samples display rhombohedral $R\bar{3}c$ symmetry (Figure 1a). Unit-cell a and c parameters,

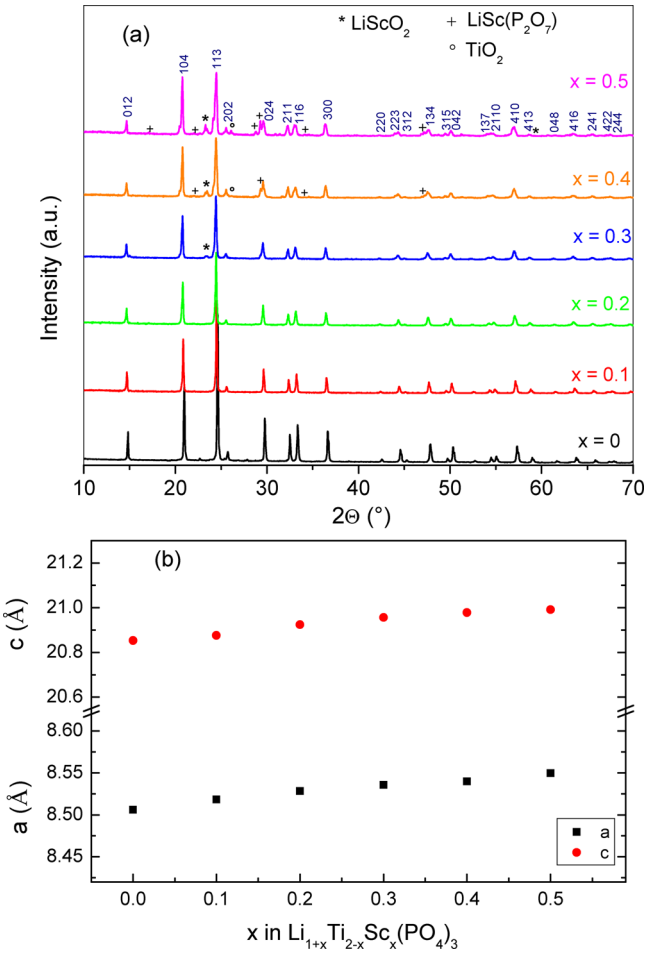

Figure 1. (a) X-ray powder diffraction patterns and (b) compositional dependence of unit-cell parameters of $Li_{1+x}Ti_{2-x}Sc_x(PO_4)_3$ samples.

determined with the Fullprof program (Le Bail method),[27] increase with the Sc content (Figure 1b). In poor Li samples, single NASICON phases are obtained; but above $x = 0.3$, secondary $LiScO_2$ (JCDPS No. 075-1743), $LiSc(P_2O_7)$ (JCDPS No. 047-0931), and TiO_2 (JCDPS No. 082-1123) phases were detected. In analyzed samples, NASICON unit-cell parameters change according to the Sc contents.[29] In Sc-rich samples, small variations detected in both parameters confirm the partial incorporation of Li and Sc in NASICON phases.

The Rietveld technique has been used to refine atom positions, thermal factors, and site occupancies (see Figure 2a). In structural refinements, the rhombohedral $LiTi_2(PO_4)_3$ phase (JCDPS No. 035-0754) has been used as a starting model. In

DOI: 10.1021/acs.inorgchem.6b02274
Inorg. Chem. 2017, 56, 1216−1224

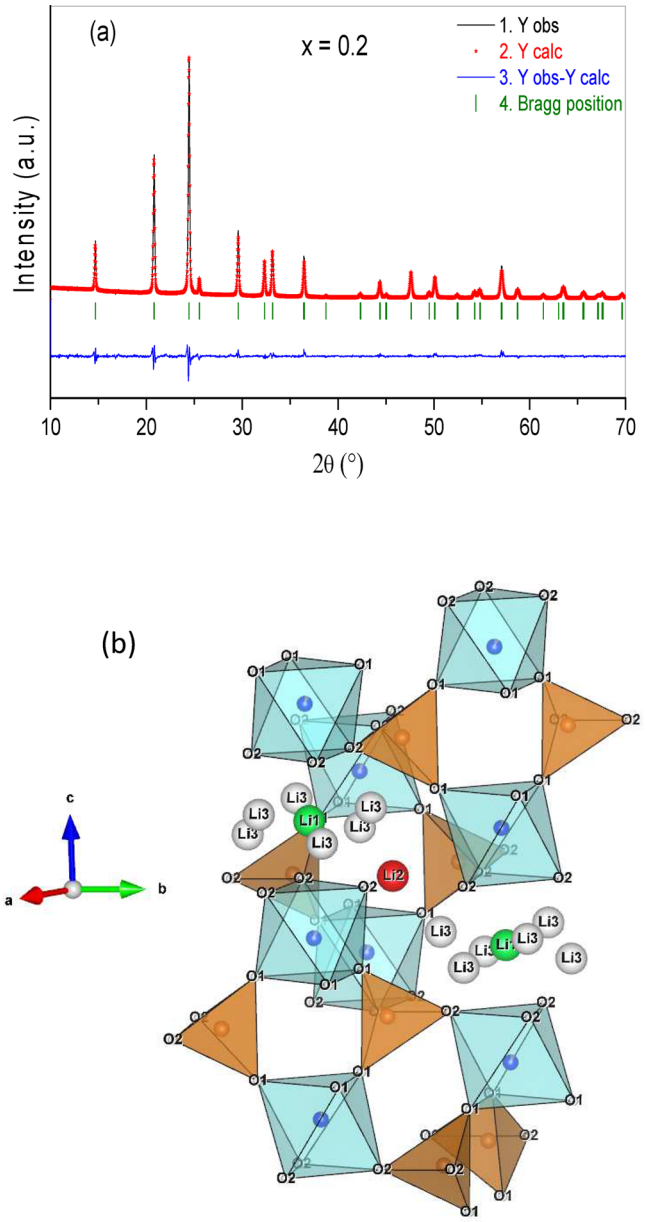

Figure 2. (a) Rietveld refinement of the $Li_{1.2}Ti_{1.8}Sc_{0.2}(PO_4)_3$ pattern recorded at room temperature. In this figure, calculated and observed profiles are included. The difference between these profiles is shown underneath. (b) Part of the $Li_{1.2}Ti_{1.8}Sc_{0.2}(PO_4)_3$ crystal structure showing lithium at M1 (Li1) and M2 (Li2) sites.

Figure 2a, observed, calculated, and difference XRD patterns of $Li_{1.2}Ti_{1.8}Sc_{0.2}(PO_4)_3$ are depicted as an example. In Li-poor ($x \leq 0.3$) samples, agreement R_p factors range between 9.5% and 13.4%, R_{wp} between 8.1% and 12.1%, R_F between 2.1% and 4.9%, and χ^2 between 1.5 and 2.2. However, In Li-rich samples ($x > 0.3$), figures of merit become worse (R_p 23.8−29.7%, R_{wp} 22.9−28.4%, R_F 10.1−12.9%, and χ^2 4.0−4.9), suggesting the presence of other secondary phases. However, XRD refinements with diphosphate $LiSc(P_2O_7)$ and NASICON phases do not significantly improve the refinements, requiring the incorporation of other phases (Figure 1a).

In NASICON phases, the substitution of Ti^{4+} by Sc^{3+} ions is compensated by additional Li^+ ions. However, Sc contents are always lower than nominal values, indicating a limited substitution of Ti^{4+} by Sc^{3+} and Li^+ cations. In $LiTi_2(PO_4)_3$, Li ions occupy M1 (6b) sites.[18] However, in $Li_{1+x}Ti_{2-x}Sc_x(PO_4)_3$, the location of part of Li at M3 (36f) sites was required. This confirms structural results reported by Catti et al.[30] on $Li_{1.5}Fe_{0.5}Ti_{1.5}(PO_4)_3$ samples and by Arbi et al.[17] on $Li_{1+x}Ti_{2-x}Al_x(PO_4)_3$ samples, where Li ions occupy M3 besides M1 sites.

Structural informations deduced from refinements are given in Tables 1 and 2. Results deduced in $Li_{1.2}Ti_{1.8}Sc_{0.2}(PO_4)_3$ show reasonable P−O distances between 1.53(3) and 1.55(8) Å and Ti,Sc−O distances between 1.86(5) and 1.95(8) Å. The Ti,Sc−O1 distances are appreciably shorter than Ti,Sc−O2, indicating the existence of some modification on charges of O1 and O2 oxygens.[31] At room temperature, Li−O distances are between 2.22(5) and 2.25(1) Å in M1 sites, and Li3−O between 2.16(4) and 2.18(6) Å in M3 sites (Figure 2b). In the series, thermal B_{Li1} factors increase from 2.09(1) to 4.01(3), and B_{Li3} from 1.11(3) to 3.84(1), indicating a higher Li mobility in Li-rich samples.

2. NMR. *^{45}Sc MAS NMR.* ^{45}Sc (I = 7/2) MAS NMR spectra of $Li_{1+x}Ti_{2-x}Sc_x(PO_4)_3$ ($0 \leq x \leq 0.5$) samples are formed by seven nuclear transitions modulated by spinning sidebands (ssb). The central component at 17.5 ppm was ascribed to octahedral Sc in NASICON compounds (Figure 3). In samples with $x \geq 0.3$, a new component was detected at 11 ppm, whose intensity increases with Sc content. The detection of two Sc environments could be ascribed to (1) phases with different composition or (2) different arrangements of Li ions in the same NASICON phase. On the basis of XRD results, the detection of secondary $LiScO_2$ and $LiScP_2O_7$ phases confirms the first option.

^{31}P MAS NMR. ^{31}P (I = 1/2) MAS NMR spectra of the $Li_{1+x}Ti_{2-x}Sc_x(PO_4)_3$ ($0 \leq x \leq 0.5$) samples are given in Figure 4. In the $LiTi_2(PO_4)_3$ sample, only one component is detected, at −27.6 ppm, ascribed to P atoms (18e sites) surrounded by four TiO_6 octahedra. For Sc-doped NASICONS, this component shifts to more positive values and becomes asymmetrically broadened, indicating the presence of additional

Table 1. Structural Parameters of $Li_{1.2}Ti_{1.8}Sc_{0.2}(PO_4)_3$ Deduced from Rietveld Refinements[a]

Atom	Wyckoff position	x	y	z	B	occupancy
Li1 (M1)	6b	0	0	0	2.49(8)	1.04(7)
Li3 (M3)	36f	0.069(2)	0.325(1)	0.071(2)	1.71(4)	0.14(1)
Ti	12c	0	0	0.141(2)	0.31(6)	1.79(2)
Sc	12c	0	0	0.141(2)	0.31(6)	0.21(9)
P	18e	0.289(6)	0	1/4	0.51(1)	3
O_1	36f	0.178(5)	0.989(6)	0.188(2)	1.17(5)	6
O_2	36f	0.183(6)	0.161(3)	0.079(4)	0.98(3)	6

[a] a = 8.527(2) Å, c = 20.924(1) Å, V = 1317.5(5) Å^3, R_B = 3.36, R_F = 2.64, R_p = 9.50, R_{WP} = 8.10%, χ^2 = 1.55.

DOI: 10.1021/acs.inorgchem.6b02274
Inorg. Chem. 2017, 56, 1216−1224

Table 2. Interatomic Li1/Li3−O, Ti,Sc−O, and P−O Distances (Å) and O−Li1/Li3−O, O−Ti,Sc−O, and O−P−O Angles (deg), Deduced from Structural Refinements of $Li_{1+x}Ti_{2-x}Sc_x(PO_4)_3$ Samples

	x = 0.1	x = 0.2	x = 0.3	x = 0.4	x = 0.5
Li1 (M1)−O_2	2.22(5)	2.22(7)	2.25(1)	2.29(7)	2.32(5)
Li3 (M3)−O_2	2.16(4)	2.16(7)	2.18(6)	2.24(8)	2.28(2)
Ti,Sc−O_1	1.86(7)	1.86(9)	1.86(5)	1.88(9)	1.92(2)
Ti,Sc−O_2	1.95(4)	1.95(6)	1.95(8)	1.96(6)	1.98(9)
P−O_1	1.54(5)	1.55(5)	1.55(8)	1.55(8)	1.56(2)
P−O_2	1.53(3)	1.53(3)	1.53(5)	1.54(4)	1.55(5)
O_2−Li1−O_2	70.1(2)	70.2(8)	69.8(2)	69.26(7)	68.92(7)
O_2−Li3−O_2	70.1(2)	69.7(2)	69.9(9)	68.3(7)	68.3(9)
O_1−Ti,Sc−O_1	94.0(1)	94.1(3)	95.5(2)	95.5(2)	96.9(6)
O_2−Ti,Sc−O_2	83.3(9)	83.2(7)	84.5(2)	86.1(9)	87.3(2)
O_1−P−O_1	110.2(7)	110.2(1)	111.9(7)	113.5(1)	115.2(6)
O_2−P−O_2	109.8(7)	108.9(9)	109.3(3)	110.4(9)	111.9(2)

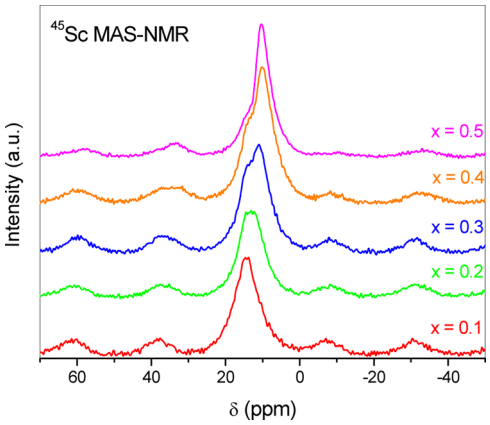

Figure 3. ^{45}Sc MAS NMR spectra of $Li_{1+x}Ti_{2-x}Sc_x(PO_4)_3$ samples.

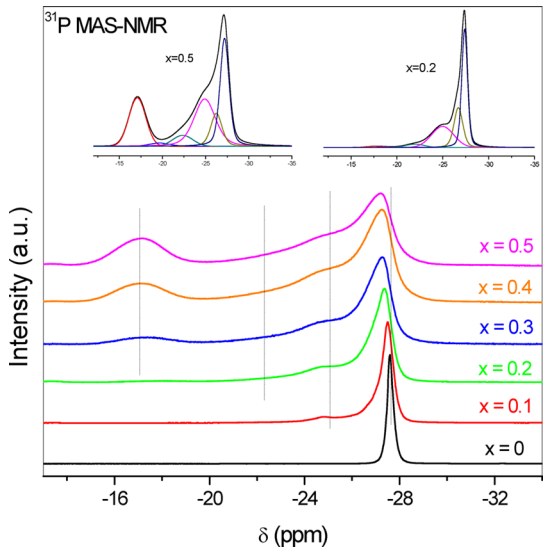

Figure 4. ^{31}P MAS NMR spectra of $Li_{1+x}Ti_{2-x}Sc_x(PO_4)_3$ samples. The deconvolutions of x = 0.2 and x = 0.5 compositions are given at the top of the figure.

components. For Sc-rich compositions, a new component detected at ∼−17 ppm was ascribed to the $LiScP_2O_7$ phase.

The deconvolutions of ^{31}P MAS NMR spectra of x = 0.2 and x = 0.5 compositions are given as examples in the insets of Figure 4. The absence of important peaks ascribed to secondary phases in XRD patterns suggests that amorphous phases could have been formed. Finally, the formation of more condensed phases, like $Sc(PO_3)_3$, must be disregarded because of the absence of peaks between −37.5 and −43 ppm.[32]

The random distribution of Ti and Sc at rhombohedral NASICON phases could produce five $P(OTi)_{4-n}(OSc)_n$ environments, with n = 0−4.[19,23] According to this, ^{31}P MAS NMR spectra of $Li_{1+x}Ti_{2-x}Sc_x(PO_4)_3$ samples have been fitted with three equally spaced $P(OTi)_4$, $P(OTi)_3(OSc)_1$, and $P(OTi)_2(OSc)_2$ components, its intensity changing with scandium content. The analysis performed here does not support the presence of NASICON phases with lower symmetry.

The quantitative analysis of the ^{31}P MAS NMR spectrum of $Li_{1.5}Ti_{1.5}Sc_{0.5}(PO_4)_3$ permitted an estimation of phosphorus incorporated in NASICON (79%) and secondary phases (21%) (Figure 5a). In general, the amount of phosphorus incorporated in secondary phases increases with Sc content. The quantitative analysis of NMR components has also permitted an estimation of relative Ti and Sc contents (Figure 5b) in NASICON phases (see Discussion section).

^{6}Li/^{7}Li MAS NMR. ^{7}Li (I = 3/2) and ^{6}Li (I = 1) MAS NMR spectra of analyzed samples are given in Figure 6a and b.^{7}Li MAS NMR spectra are composed by central (+1/2 ⇄ −1/2) and external (−3/2 ⇄ −1/2) and (+1/2 ⇄ + 3/2) transitions, modulated by equally spaced ssb's. The central transition of ^{7}Li MAS NMR spectra is located near −1.2 ppm, shifting toward more positive values as the Sc content increases (inset of Figure 6a). When secondary phases are formed, a broad component at ∼0 ppm is detected (x = 0.4 and 0.5 samples). In secondary phases, the mobility of Li is very low, reducing considerably ion conductivity in the prepared samples. Chemical shifts values (δ_{iso}) and quadrupolar constants (C_Q and η) of different ^{7}Li NMR components are depicted in Table 3.

In ^{6}Li MAS NMR spectra of $Li_{1+x}Ti_{2-x}Sc_x(PO_4)$ samples, only central transitions are detected as a consequence of lower quadrupolar interactions between Li ions and the NASICON network (Figure 6b). In ^{6}Li MAS NMR spectra, the main component was located near −1.2 ppm, shifting toward more positive values as the Sc content increases. The shift and broadening observed in this component suggest the presence of two components, which could be associated with Li ions at the M1 and M3 positions. Below x = 0.2, the line width remains small, indicating that Li ions display high mobility in the NASICON phases. In secondary phases, lower mobility of lithium increases the number of spinning sidebands, decreasing the intensity detected in the central ^{7}Li MAS NMR component.

DOI: 10.1021/acs.inorgchem.6b02274
Inorg. Chem. 2017, 56, 1216−1224

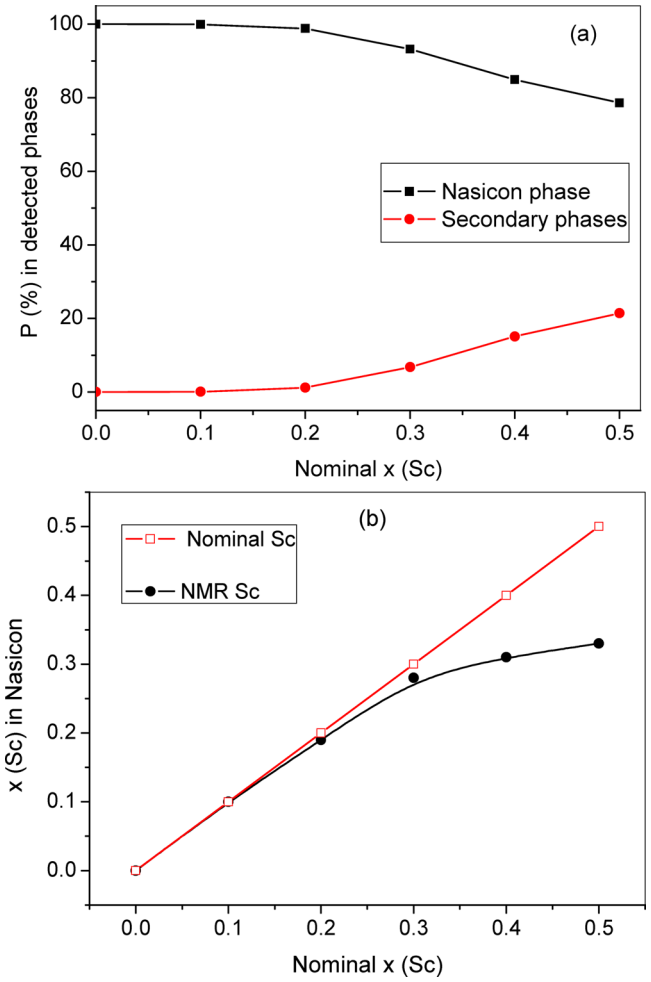

Figure 5. (a) Phosphorus (%) in NASICON and secondary phases as a function of the nominal x (Sc). (b) Scandium (x) content in NASICON phases as a function of nominal values.

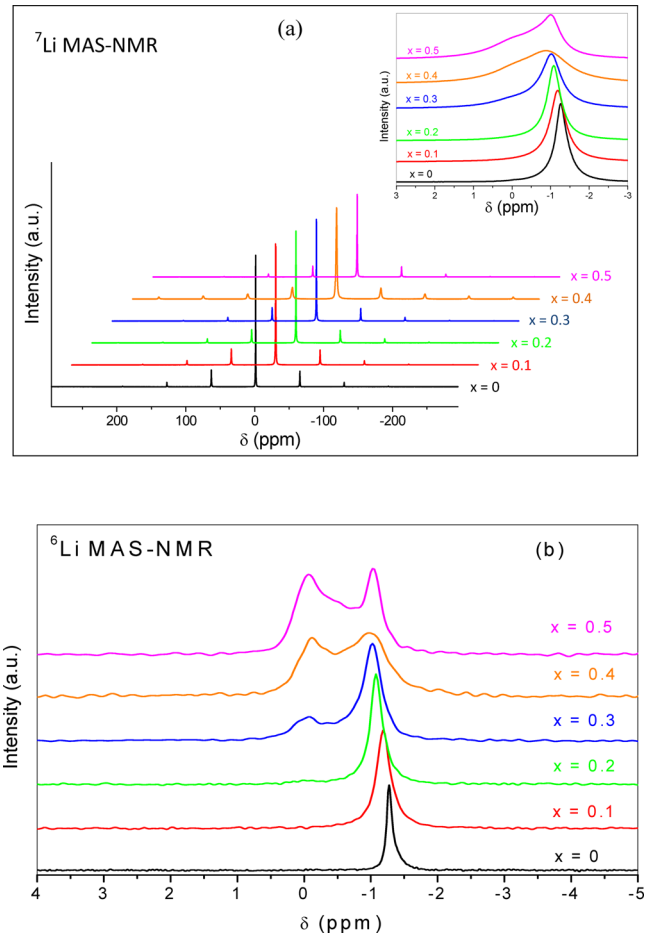

Figure 6. (a) ^{7}Li and (b) ^{6}Li MAS NMR spectra of $Li_{1+x}Ti_{2-x}Sc_x(PO_4)_3$ samples. In ^{7}Li-MAS NMR spectra spinning side bands are clearly identified.

From this fact, relative intensities of Li components are different in ^{6}Li and ^{7}Li MAS NMR spectra, requiring the consideration of spinning side bands in the ^{7}Li NMR spectra quantification (Figure 6a and b).

3. ELECTRICAL PROPERTIES

Figure 7 displays room-temperature Nyquist ($-Z''$ versus Z') plots of $Li_{1.2}Ti_{1.8}Sc_{0.2}(PO_4)_3$ samples. In this figure, the equivalent circuit used for data analysis is given as an inset. From impedance plots, it has been possible to deduce by complex nonlinear least-squares fittings "bulk", grain-boundary, and electrode contributions to conductivity.[33]

In Figure 8a, the frequency dependence of the real part of Li conductivity is given for $Li_{1+x}Ti_{2-x}Sc_x(PO_4)_3$ ($0 \le x \le 0.5$) samples. The increment of Li content enhances Li mobility, shifting the crossover frequency between ac and dc "bulk" contributions toward higher frequency.[34] To better analyze bulk conductivity, we extended the frequency range from 10^2 Hz to 3×10^9 Hz. The relaxation from "bulk" to "grain boundary" responses passes through a maximum in derivative plots (Figure 8b). The ideal response should display derivative values of dc conductivity close to zero for "bulk" or "grain boundary" contributions. In the $x = 0.1$ sample the derivative plot is similar to that deduced from the ideal behavior; but the "dc-bulk" derivative values are near 0.22, which is close to the values reported in other Li-NASICON ceramic samples.[35] In the $x = 0.2$ sample, besides "bulk" and "grain boundary" responses, a new small response is detected between both contributions, which increases with Sc content (arrows in Figure 8a and b). This response has been previously ascribed to "core−shell" structures.[36]

In Figure 9a, bulk and overall conductivity of the $Li_{1+x}Ti_{2-x}Sc_x(PO_4)_3$ ($0 \le x \le 0.5$) samples are plotted versus reciprocal temperature ($1000/T$). In all samples, dc conductivity values were fitted to the Arrhenius expression:

$$\sigma_{dc}T = A_0 \exp(-E_a/k_BT) \quad (1)$$

where σ_{dc} stands for dc conductivity, A_0 for pre-exponential factors, E_a for activation energy, k_B for the Boltzmann constant, and T for absolute temperature (K). Activation energy and pre-exponential factors of $Li_{1+x}Ti_{2-x}Sc_x(PO_4)_3$ samples are listed in Table 4. Activation energy deduced from total and bulk conductivities displays similar trends; however, bulk values are always higher than overall ones. Activation energy values display a minimum at $x = 0.2$ (Figure 9b).

IV. DISCUSSION

The combined XRD, NMR, and IS analysis permitted a deeper analysis of structure and electrical properties of rhombohedral (space group $R\bar{3}c$) $Li_{1+x}Ti_{2-x}Sc_x(PO_4)_3$ samples.

DOI: 10.1021/acs.inorgchem.6b02274
Inorg. Chem. 2017, 56, 1216−1224

Table 3. Chemical Shift δ_{iso} (ppm) Values Deduced from ^{7}Li and ^{31}P MAS-NMR Spectra of $Li_{1+x}Ti_{2-x}Sc_x(PO_4)_3$ and $LiScP_2O_7$ Phases[a]

Sc_x	Sc_x^{NMR}	$\delta(P(OTi)_4)$	$\delta(P(OTi)_3(OSc)_1)$	$\delta(P(OTi)_2(OSc)_2)$	$\delta(P(OTi)_1(OSc)_3)$	$\delta(LiScP_2O_7)$	$\delta Li^{(1)}$	$\delta Li^{(2)}$	$C_Q^{(1)}$	$C_Q^{(2)}$
0.0	0.0	−27.61					−1.28		43	
0.1	0.10	−27.50/−27.00	−24.94	−22.30	−19.65		−1.18		40	
0.2	0.19	−27.35/−26.70	−25.00	−22.40	−19.65		−1.10		36	
0.3	0.28	−27.35/−26.52	−24.8	−22.45	−19.46	−17.22	−1.08	0.11	46	71
0.4	0.31	−27.20/−26.35	−24.50	−22.20	−19.60	−17.07	−1.00	0.13	49	85
0.5	0.33	−27.19/−26.25	−24.9	−22.35	−19.65	−17.09	−1.21	0.17	52	97

[a]Quadrupolar constant C_Q (kHz) deduced from ^{7}Li MAS-NMR spectra of NASICON and secondary phases.

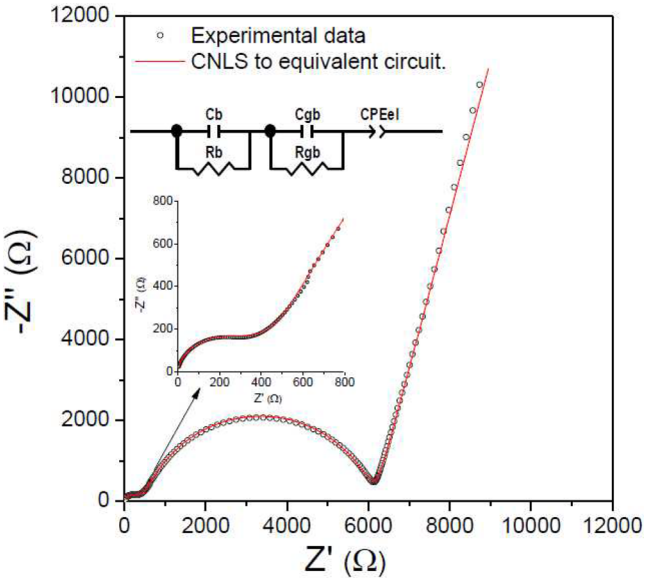

Figure 7. Nyquist diagrams of the $Li_{1.2}Ti_{1.8}Sc_{0.2}(PO_4)_3$ sample at room temperature. The equivalent circuit used in fitting of data is given as an inset.

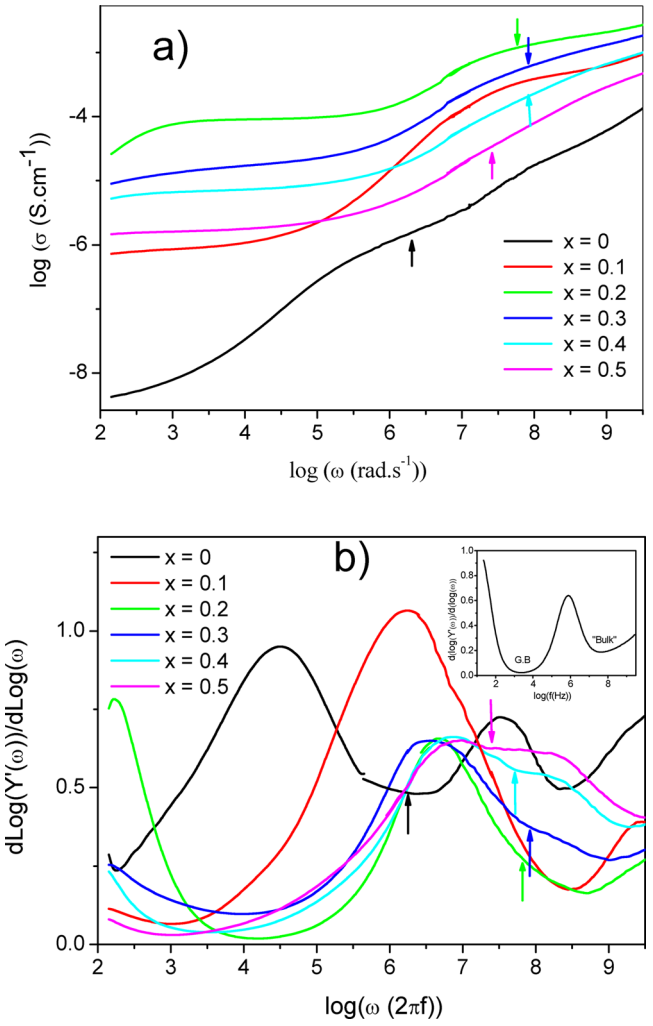

Figure 8. (a) RT real conductivity versus angular frequency in $Li_{1+x}Ti_{2-x}Sc_x(PO_4)_3$ samples. (b) Frequency derivative of admittance plots. The inset shows the simulated derivative of an ideal solid electrolyte ceramic.

Lattice *a* and *c* parameters increase with Sc content (Figure 1b) as a consequence of bigger Sc^{3+} (0.74 Å) than Ti^{4+} (0.60 Å) radius.[29] For $x \geq 0.3$ samples, a lower variation of unit-cell parameters (slope) was detected, suggesting a lower incorporation of Sc in NASICON phases. This observation agrees with detection of additional phases in XRD and ^{31}P and ^{7}Li MAS NMR spectra.

In the $Li_{1+x}Ti_{2-x}Sc_x(PO_4)_3$ series, Ti^{4+} is substituted by Sc^{3+}+Li^{+}, increasing the amount of lithium. In ^{31}P MAS NMR spectra of rhombohedral phases, substitution of Ti by Sc should produce five equally spaced components, associated with 4Ti, 3Ti1Sc, 2Ti2Sc, 1Ti3Sc, and 4Sc environments; however, the substitution of Ti^{4+} by Sc^{3+} cations produces only the three first components. From the intensity of these components, the chemical composition of samples was estimated with the expression[23,24]

$$Sc^{3+}/Ti^{4+} = \frac{4I_4 + 3I_3 + 2I_2 + I_1}{I_3 + 2I_2 + 3I_1 + 4I_0} \quad (2)$$

where I_n stands for relative intensity of ^{31}P NMR components associated with nSc·$(4-n)$ Ti environments.

From Sc^{3+}/Ti^{4+}ratios, octahedral Sc^{3+} (x) or Ti^{4+} $(2-x)$ contents were deduced, using the expression

$$Sc^{3+}/Ti^{4+} = \frac{x}{2-x} \quad (3)$$

Sc contents deduced from ^{31}P MAS NMR spectra (Table 3) are always lower than nominal ones (Figure 5b). In particular, important differences were detected in Sc-rich $x = 0.4$ and 0.5 samples, where secondary $LiScO_2$ and $LiScP_2O_7$ phases were detected in XRD patterns. Taking into account that XRD patterns of Sc-poor samples are basically formed by rhombohedral $R\bar{3}c$ patterns of NASICON phases, the ^{45}Sc MAS NMR peak detected at ~17.5 ppm was ascribed to $Li_{1+x}Ti_{2-x}Sc_x(PO_4)_3$ and that at 11 ppm to Sc ions in the $LiScP_2O_7$ phase.

DOI: 10.1021/acs.inorgchem.6b02274
Inorg. Chem. 2017, 56, 1216−1224

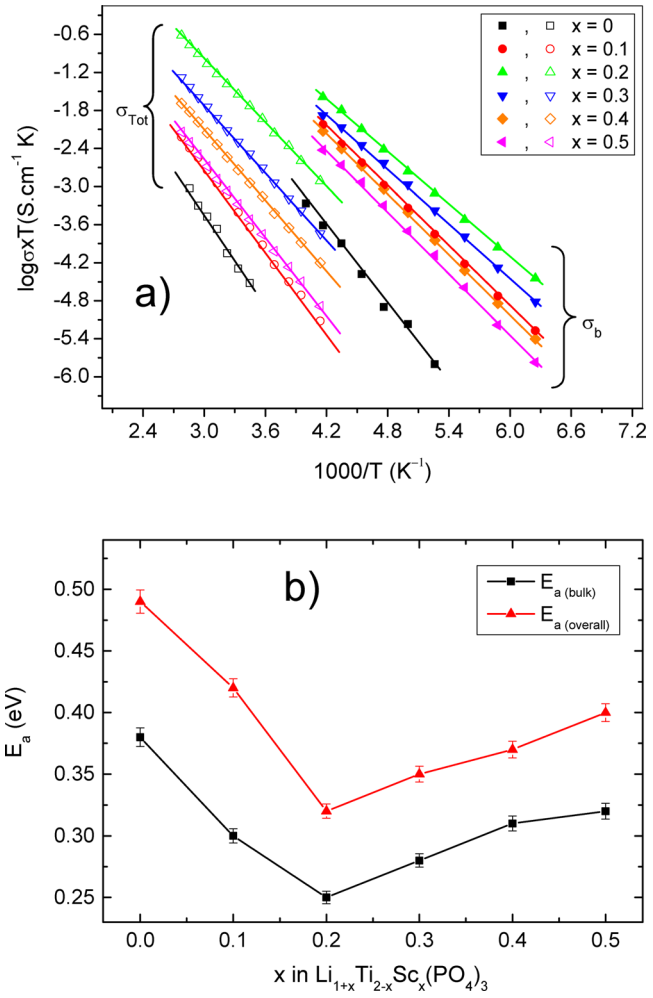

Figure 9. (a) Bulk (closed symbols) and overall (open symbols) dc conductivities versus reciprocal temperature. (b)Variation of activation energy as a function of the Sc content in $Li_{1+x}Ti_{2-x}Sc_x(PO_4)_3$ samples.

Taking into account the amount of phosphorus in the NASICON phase (Figure 5a) and that of scandium incorporated in the $Li_{1-x}Ti_{2-x}Sc_x(PO_4)_3$ structure (Figure 5b), it is possible to deduce, by subtraction from nominal compositions, the average chemical composition of the remaining phases. In the case of $x = 0.5$, chemical compositions of detected phases can be given as $0.79Li_{1.33}Ti_{1.67}Sc_{0.33}(PO_4)_3$ (NASICON) + $0.21Li_{2.15}Ti_{0.86}Sc_{1.13}P_{3.00}O_{12.02}$ (remaining phase), where the remaining composition should correspond again to a Li-rich NASICON phase. If the maximum Li content incorporated into NASICONs is 1.35/formula, the remaining composition cannot exist as a particular phase. From this fact, the presence of more stable $LiScO_2$, $LiScP_2O_7$, and TiO_2 must be produced. These phases explain the presence of additional phases in ^{45}Sc, ^{31}P, and ^{7}Li MAS NMR spectra. The limited incorporation of Sc in NASICON phases makes the determination of the maximum Sc incorporated an important factor in optimization of electric properties of prepared ceramics.

Li Mobility. *Samples with $x < 0.3$.* Due to large Li conductivity, an enlargement of the frequency ranges was required to analyze bulk conductivity of NASICON phases (Figure 8a). To better differentiate bulk and grain-boundary contributions, frequency derivative plots of conductivity have been used (Figure 8b).[33]

The ^{7}Li MAS NMR spectrum of $LiTi_2(PO_4)_3$ indicates that Li ions occupy M1 sites at ternary axes as deduced from quadrupolar information ($\eta = 0$, axial symmetry).[25] When the Li content increases in $Li_{1+x}Ti_{2-x}Sc_x(PO_4)_3$ samples, electrostatic repulsions between Li ions favor occupation of M3 sites. The delocalization of lithium in conduction···Li1−Li3−Li1··· channels is favored by creation of vacant sites at the intersection of conduction paths (M1 sites).[17] In Li-poor NASICON samples, the Li NMR component was centered at −1.2, but in some Li-rich phases, a second component was detected at −0.8 ppm, making difficult a separated analysis of two components in analyzed samples. Both components were associated with Li at M1 and M3 sites. According to this, the line width of the Li NMR signal should increase up to $x = 0.2$; however, exchange processes between adjacent M1 and M3 sites reduce line widths of the resulting components (Figure 6a and b). This explains that overall conductivity increases when the amount of scandium and lithium increases up to $x = 0.2$ (Figure 8 and Table 4).

Activation energy values display the opposite trend of that reported for conductivity. The incorporation of Sc in $LiTi_2(PO_4)_3$ reduces both "bulk" and the grain boundary activation energy of the Ti end member of the series (0.38 and 0.49 eV). The "bulk" activation energy further decreases from 0.30 to 0.25 eV and the "grain boundary" from 0.42 to 0.32 eV when Sc content increases from 0.1 to 0.2 in $Li_{1+x}Ti_{2-x}Sc_x(PO_4)_3$ samples. Above $x = 0.2$, Li conductivity decreases and activation energies increase because of secondary phases formed at the NASICON particle surface.

From Arrhenius plots of dc conductivities, it was possible to extrapolate pre-exponential A_0 terms of conductivity (Table 4). In $Li_{1+x}Ti_{2-x}Sc_x(PO_4)_3$, vacancy disordering increases, decreasing considerably pre-exponential A_0 factors with the Li content. The sample $Li_{1.2}Ti_{1.8}Sc_{0.2}(PO_4)_3$ displays one of the best reported ion conductivities in NASICON compounds and other ion conductors.[37] The maximum of bulk conductivity detected here was similar to that reported elsewhere.[20,21]

Table 4. Activation Energy (E_a) and Pre-exponential Factor (A_0) Deduced from Bulk, and Overall Conductivities (σ) Measured at 298 K in $Li_{1+x}Ti_{2-x}Sc_x(PO_4)_3$ Samples

	bulk conductivity			overall conductivity		
Sc_x	σ (S·cm^{-1})	A_0 (S·cm^{-1})	E_a (eV)	σ (S·cm^{-1})	A_0 (S·cm^{-1})	E_a (eV)
0.0	7.61×10^{-6}	3.01×10^{4}	0.38	2.04×10^{-7}	1.10×10^{4}	0.49
0.1	3.89×10^{-4}	2.88×10^{4}	0.30	1.30×10^{-6}	5.34×10^{3}	0.42
0.2	2.51×10^{-3}	5.33×10^{3}	0.25	9.98×10^{-5}	8.38×10^{3}	0.32
0.3	7.91×10^{-4}	1.34×10^{4}	0.28	2.68×10^{-5}	4.90×10^{3}	0.35
0.4	1.99×10^{-4}	3.23×10^{4}	0.31	6.09×10^{-6}	3.42×10^{3}	0.37
0.5	9.74×10^{-5}	2.57×10^{4}	0.32	1.86×10^{-6}	2.96×10^{3}	0.40

DOI: 10.1021/acs.inorgchem.6b02274
Inorg. Chem. 2017, 56, 1216−1224

Samples with $x \geq 0.3$. As shown Table 4, the overall conductivity decreases and activation energy increases with Sc content for samples with $x > 0.2$. The observed variation does not agree with the monotonic increment of the unit-cell volume, suggesting that other factors affect the conductivity. The derivative values associated with the "bulk" conductivity increase with Sc content, displaying 0.27, 0.36, and 0.40 values in $x = 0.3$, 0.4, and 0.5 samples, respectively. High values of the "dc-bulk" derivative are ascribed to the formation of secondary non-well-crystallized phases. The formation of disordered Li/Sc oxides or diphosphates at NASICON particles (core−shell structures) decreases the amount and mobility of lithium in samples. In agreement with these results, the quantitative analysis of ^{31}P MAS NMR spectra of NASICON phases shows lower Sc/Ti values than nominal ones (Table 3 and Figure 5b). The results obtained in this work differ slightly from those obtained in samples prepared by the sol−gel process.[22] The new broad component detected at 0 ppm in Li MAS NMR spectra must correspond to secondary phases that increase the grain-boundary contribution.

V. CONCLUSIONS

The $Li_{1+x}Ti_{2-x}Sc_x(PO_4)_3$ ($0 \leq x \leq 0.5$) series has been prepared by solid-state reaction and characterized with XRD, NMR, and IS techniques. In Sc-poor samples, XRD patterns display only NASICON phases with rhombohedral symmetry (space group $R\bar{3}c$). In Sc-rich samples, secondary, $LiScO_2$, $LiScP_2O_7$, and TiO_2 phases coexist with the NASICON phase.

In $x < 0.3$ samples, the substitution of Ti^{4+} by Sc^{3+} increases the Li content, enhancing electrostatic Li−Li repulsions, favoring the creation of vacant M1 sites. This arrangement of vacancy increases Li conductivity; however, the formation of the secondary $LiScO_2$ and $LiScP_2O_7$ phases decreases the amount of Li and Sc incorporated in the NASICON phase. In parallel to the phases segregation, the formation of core−shell structures reduces the total conductivity of $x > 0.3$ samples. From this fact, the determination of cation miscibility in the NASICON $Li_{1+x}Ti_{2-x}Sc_x(PO_4)_3$ series was of major importance in optimization of transport properties. This miscibility seems to be related to the preparation method used.

High conductivity values found in the $Li_{1+x}Ti_{2-x}Sc_x(PO_4)_3$ series open new perspectives for preparing NASICON-based electrolytes for all-solid-state lithium batteries. At present, electrical properties of $Li_{1.2}Ti_{1.8}Sc_{0.2}(PO_4)_3$ make this material one of the best reported ion conductors at room temperature ($\sigma_b \approx 2.5 \times 10^{-3}$ S·cm^{-1}), displaying one of the lowest activation energies reported in NASICON compounds (0.25 eV).

AUTHOR INFORMATION

Corresponding Author

*E-mail: k.arbi@tudelft.nl; rbikml@gmail.com.

ORCID

Kamel Arbi: 0000-0002-4630-438X

Notes

The authors declare no competing financial interest.

ACKNOWLEDGMENTS

R.K. would like to thank the Tunisian Ministry of Higher Education and Scientific Research for financial support. This work was funded by Spanish MINECO MAT2013-46452-C4-2R and MATERYENER3-CAM (S2013/MIT-2753) projects and the European NANOLICOM (FP7-PEOPLE-2009-IRSES) project.

REFERENCES

(1) Goodenough, J. B.; Hong, H. Y. P.; Kafalas, J. Fast Na^+-ion transport in skeleton structures. *Mater. Res. Bull.* **1976**, *11*, 203−220.

(2) Gopalakrishnan, J.; Shukla, A. K.; Thangadurai, V. Rational design of solid materials - A case study of lithium-ion conductors. *Curr. Sci.* **1999**, *76*, 1473−1480.

(3) Aono, H.; Imanaka, N.; Adachi, G. Y. High Li^+ Conducting Ceramics. *Acc. Chem. Res.* **1994**, *27*, 265−270.

(4) Fergus, J. W. Ceramic and polymeric solid electrolytes for lithium-ion batteries. *J. Power Sources* **2010**, *195*, 4554−4569.

(5) Imanishi, N.; Yamamoto, O. Rechargeable lithium−air batteries: characteristics and prospects. *Mater. Today* **2014**, *17*, 24−30.

(6) Takada, K. Progress and prospective of solid-state lithium batteries. *Acta Mater.* **2013**, *61*, 759−770.

(7) Anantharamulu, N.; Koteswara Rao, K.; Rambabu, G.; Kumar, B. V.; Radha, V.; Vithal, M. A wide-ranging review on Nasicon type materials. *J. Mater. Sci.* **2011**, *46*, 2821−2837.

(8) Mykhailo, M.; Thomas, H.; Anatoliy, S.; Hans, B.; Dmitry, C.; Thomas, H.; Karl, G. S.; Ethel, C. B.; Michael, J. H.; Helmut, E. Lithium Diffusion Pathway in $Li_{1.3}Al_{0.3}Ti_{1.7}(PO_4)_3$ (LATP) Superionic Conductor. *Inorg. Chem.* **2016**, *55*, 2941−2945.

(9) Alami, M.; Brochu, R.; Soubeyroux, J. L.; Graverau, P.; Le Flem, G.; Hagenmuller, P. J. Structure and thermal expansion of $LiGe_2(PO_4)_3$. *J. Solid State Chem.* **1991**, *90*, 185−193.

(10) Paris, M. A.; Martinez-Juarez, A.; Rojo, J. M.; Sanz, J. Lithium mobility in the NASICON-type compound $LiTi_2(PO_4)_3$ by nuclear magnetic resonance and impedance spectroscopies. *J. Phys.: Condens. Matter* **1996**, *8*, 5355−5366.

(11) Catti, M.; Stramare, S.; Ibberson, R. Lithium location in NASICON-type Li^+ conductors by neutron diffraction. I. Triclinic α'-$LiZr_2(PO_4)_3$. *Solid State Ionics* **1999**, *123*, 173−180.

(12) Losilla, E. R.; Aranda, M. A. G.; Martinez-Lara, M.; Bruque, S. Reversible triclinic-rhombohedral phase transition in $LiHf_2(PO_4)_3$: Crystal structures from neutron powder diffraction. *Chem. Mater.* **1997**, *9*, 1678−1685.

(13) Morin, E.; Angenault, J.; Couturier, J. C.; Quarton, M.; He, H.; Klinowski, J. Phase-transition and crystal-structures of $LiSn_2(PO_4)_3$. *Eur. J. Solid State Inorg. Chem.* **1999**, *34*, 947−958.

(14) Aono, H.; Sugimoto, E.; Sadaoka, Y.; Imanoka, N.; Adachi, G. Ionic Conductivity of Solid Electrolytes Based on Lithium Titanium Phosphate. *J. Electrochem. Soc.* **1990**, *137*, 1023−1027.

(15) Tran Qui, D.; Hamdoune, S.; Soubeyroux, J. L.; Prince, E. Neutron powder diffraction study of solid solution $Li_{1+x}Ti_{2-x}In_xP_3O_{12}$: I. $0.0 \leq x \leq 0.4$. *J. Solid State Chem.* **1988**, *72*, 309−315.

(16) Best, A. S.; Forsyth, M.; MacFarlane, D. R. Stoichiometric changes in lithium conducting materials based on $Li_{1+x}AlxTi_{2-x}(PO_4)_3$: impedance, X-ray and NMR studies. *Solid State Ionics* **2000**, *136*, 339−344.

(17) Arbi, K.; Hoelzel, M.; Kuhn, A.; García-Alvarado, F.; Sanz, J. Structural Factors That Enhance Lithium Mobility in Fast-Ion $Li_{1+x}Ti_{2-x}Al_x(PO_4)_3$ ($0 \leq x \leq 0.4$) Conductors Investigated by Neutron Diffraction in the Temperature Range 100−500 K. *Inorg. Chem.* **2013**, *52*, 9290−9296.

(18) Chandran, C. V.; Pristat, S.; Witt, E.; Tietz, F.; Heitjans, P. Solid-State NMR Investigations on the Structure and Dynamics of the Ionic Conductor $Li_{1+x}Al_xTi_{2-x}(PO_4)_3$ ($0.0 \leq x \leq 1.0$). *J. Phys. Chem. C* **2016**, *120*, 8436−8442.

(19) Arbi, K.; Lazarraga, M. G.; Ben Hassen Chehimi, D.; Ayadi-Trabelsi, M.; Rojo, J. M.; Sanz, J. Lithium Mobility in $Li_{1.2}Ti_{1.8}R_{0.2}(PO_4)_3$ Compounds (R = Al, Ga, Sc, In) as Followed by NMR and Impedance pectroscopy. *Chem. Mater.* **2004**, *16*, 255−262.

(20) Pérez-Estébanez, M.; Isasi-Marín, J.; Többens, D. M.; Rivera-Calzada, A.; León, C. A systematic study of Nasicon-type $Li_{1+x}M_xTi_{2-x}(PO_4)_3$ (M: Cr, Al, Fe) by neutron diffraction and impedance spectroscopy. *Solid State Ionics* **2014**, *266*, 1−8.

DOI: 10.1021/acs.inorgchem.6b02274
Inorg. Chem. 2017, 56, 1216−1224

(21) Kazuaki, A.; Yuria, S.; Takashi, A.; Hiroyuki, K.; Nakamura, O. Li^+-ion conductivity of $Li_{1+x}M_xTi_{2-x}(PO_4)_3$ (M: Sc^{3+}, Y^{3+}). *Solid State Ionics* **1992**, *53*, 723−727.
(22) Salkus, T.; Barre, M.; Kazionis, A.; Kazakevicius, E.; Bohnke, O.; Selskiene, A. Ionic conductivity of $Li_{1.3}Al_{0.3-x}Sc_xTi_{1.7}(PO_4)_3$ (x = 0, 0.1, 0.15, 0.2, 0.3) solid electrolytes prepared by Pechini process. *Solid State Ionics* **2012**, *225*, 615−619.
(23) Arbi, K.; Jimenez, R.; Šalkus, T.; Orliukas, A. F.; Sanz, J. On the influence of the cation vacancy on lithium conductivity of $Li_{1+x}R_xTi_{2-x}(PO_4)_3$ Nasicon type materials. *Solid State Ionics* **2015**, *271*, 28−33.
(24) Losilla, E. R.; Aranda, M. A. G.; Bruque, S.; Paris, M. A.; Sanz, J. Understanding Na mobility in NASICON materials: A Rietveld, ^{23}Na and ^{31}P MAS NMR, and impedance study. *Chem. Mater.* **1998**, *10*, 665−673.
(25) Paris, M. A.; Sanz, J. Structural changes at the triclinic-rhombohedral transition and their influence on the Li mobility of the fast-ion conductor $LiHf_2(PO_4)_3$. *Phys. Rev. B: Condens. Matter Mater. Phys.* **2000**, *62*, 810−817.
(26) Rietveld, H. M. A profile refinement method for nuclear and magnetic structures. *J. Appl. Crystallogr.* **1969**, *2*, 65−71.
(27) Rodriguez-Carvajal, J. Recent Advances in Magnetic Structure Determination by Neutron Powder Diffraction. *Phys. B* **1993**, *192*, 55−69.
(28) Bruker WINFIT program, *Bruker Rep.***1994**, *140*, 43.
(29) Shannon, R. D. Revised effective ionic radii and systematic studies of interatomic distances in halides and chalcogenides. *Acta Crystallogr., Sect. A: Cryst. Phys., Diffr., Theor. Gen. Crystallogr.* **1976**, *A32*, 757−767.
(30) Catti, M.; Comotti, A.; Di Blas, S.; Ibberson, R. M. Extensive lithium disorder in $Li_{1.5}Fe_{0.5}Ti_{1.5}(PO_4)_3$ Nasicon by neutron diffraction, and the $Li_{1+x}Fe_xTi_{2-x}(PO_4)_3$ phase diagram. *J. Mater. Chem.* **2004**, *14*, 835−839.
(31) Diez-Gómez, V.; Arbi, K.; Sanz, J. Modeling Ti/Ge Distribution in $LiTi_{2-x}$ Ge_x $(PO_4)_3$ NASICON Series by ^{31}P MAS NMR and First-Principles DFT Calculations. *J. Am. Chem. Soc.* **2016**, *138*, 9479−9486.
(32) Nalin, M.; Ribeiro, S. J. L.; Messaddeq, Y.; Schneider, J.; Donoso, P. Scandium fluorophosphate glasses: A structural approach. *C. R. Chim.* **2002**, *5*, 915−920.
(33) Bucheli, W.; Jimenez, R.; Sanz, J.; Várez, A. The $\log(\sigma)$ vs. $\log(\omega)$ derivative plot used to analyze the ac conductivity. Application to fast Li^+ ion conductors with perovskite structure. *Solid State Ionics* **2012**, *227*, 113−118.
(34) Jonscher, A. K. *Dielectric Relaxation in Solids*; Chelsea Dielectric Press: London, 1983.
(35) Bucheli, W.; Arbi, K.; Sanz, J.; Nuzhnyy, D.; Kamba, S.; Várez, A.; Jiménez, R. Near constant loss regime in fast ionic conductors analyzed by impedance and NMR spectroscopies. *Phys. Chem. Chem. Phys.* **2014**, *16*, 15346−15354.
(36) Arbi, K.; Bucheli, W.; Jiménez, R.; Sanz, J. High lithium ion conducting solid electrolytes based on NASICON $Li_{1+x}AlxM_{2-x}(PO_4)_3$ materials (M = Ti, Ge and $0 \leq x \leq 0.5$). *J. Eur. Ceram. Soc.* **2015**, *35*, 1477−1484.
(37) Knauth, P. Inorganic solid Li ion conductors: An overview. *Solid State Ionics* **2009**, *180*, 911−916.

DOI: 10.1021/acs.inorgchem.6b02274
Inorg. Chem. 2017, 56, 1216−1224